

THE 3-4 μ M SPECTRA OF JUPITER TROJAN ASTEROIDS

M.E. BROWN

Division of Geological and Planetary Sciences, California Institute of Technology, Pasadena, CA 91125
Draft version June 10, 2016

ABSTRACT

To date, reflectance spectra of Jupiter Trojan asteroids have revealed no distinctive absorption features. For this reason, the surface composition of these objects remains a subject of speculation. Spectra have revealed, however, that the Jupiter Trojan asteroids consist of two distinct sub-populations which differ in the optical to near-infrared colors. The origins and compositional differences between the two sub-populations remain unclear. Here we report the results from a 2.2-3.8 μ m spectral survey of a collection of 16 Jupiter Trojan asteroids, divided equally between the two sub-populations. We find clear spectral absorption features centered around 3.1 μ m in the less red population. Additional absorption consistent with expected from organic materials might also be present. No such features are seen in the red population. A strong correlation exists between the strength of the 3.1 μ m absorption feature and the optical to near-infrared color of the objects. While traditionally absorptions such as these in dark asteroids are modeled as being due to fine-grain water frost, we find it physically implausible that the special circumstances required to create such fine-grained frost would exist on a substantial fraction of the Jupiter Trojan asteroids. We suggest, instead, that the 3.1 μ m absorption on Trojans and other dark asteroids could be due to N-H stretch features. Additionally, we point out that reflectivities derived from WISE observations show a strong absorption beyond 4 μ m for both populations. The continuum of 3.1 μ m features and the common absorption beyond 4 μ m might suggest that both sub-populations of Jupiter Trojan asteroids formed in the same general region of the early solar system.

1. INTRODUCTION

The Jupiter Trojan asteroids remain mysterious in both their origins and in their compositions. As small bodies orbiting along the inner boundary of the realm of the giant planets, their histories contain important clues to the origins and evolution of the entire planetary system.

Recent proposals have suggested that the Jupiter Trojans were emplaced from the outer solar system during an early period of giant planet dynamical instability (Morbidelli et al. 2005; Nesvorný et al. 2013). In this hypothesis, the objects that are now Jupiter Trojans and the objects that are now in the Kuiper belt are derived from the same source populations but underwent different stochastic dynamical histories to lead to their very separate locations today. Jupiter Trojans are, in this view, a much more easily accessed population of the types of icy bodies inhabiting the outer solar system.

While the dynamical connection between the Jupiter Trojan and Kuiper belt source region seems promising, little progress has been made in connecting the compositions of these two sets of objects. Ices such as water and methanol have been seen on small objects in the Kuiper belt (Barucci et al. 2011; Brown et al. 2012), but reflectance spectroscopy of Jupiter Trojans has revealed nothing but featureless red spectra. These red spectra have typically been interpreted as being due to the presence of organic materials, but no such spectral signatures have ever been seen. Indeed, the only positively identified spectral features on Jupiter Trojans comes from thermal emission spectra, which show the signatures of fine-grained silicates (Emery et al. 2006). Spectral mod-

els including reddened space-weathered silicates appear to explain the visible-to-near-infrared spectra as effectively as any organic materials (Emery et al. 2011).

An important clue into the compositions of the Jupiter Trojans and perhaps into their connection with objects in the Kuiper belt is the insight that the Jupiter Trojans are a mixture of two populations with distinct (though still featureless) spectra (Emery et al. 2011). The "red" and "less red" populations differ in their optical and near-infrared colors, their infrared reflectivities measured from the WISE spacecraft, and in their size distributions (Emery et al. 2011; Grav et al. 2012; Wong et al. 2014; Wong & Brown 2015a), yet seem completely mixed dynamically. It is not known whether these two color populations represent distinct source populations, distinct dynamical pathways, distinct collision histories, or some other set of mechanisms. To date, the only hypothesis for the two populations is that they are both from the Kuiper belt source region, but the less-red objects formed in the inner part of the source region where H₂S evaporated from the surface, while the red objects retained their surface H₂S (Wong & Brown 2016). In this hypothesis, subsequent irradiation then caused significant chemical differences in the sulfur-free and sulfur-containing involatile mantles (Mahjoub et al. 2016), leading to the bifurcation of not just Jupiter Trojan colors, but also to those of the Centaurs (Tegler et al. 2008) and the small Kuiper belt objects (Fraser & Brown 2012; Wong & Brown 2015b).

To further explore the compositions of the Jupiter Trojans, to examine connections with the Kuiper belt population, and to determine differences between the two populations, we have obtained 2.2-3.8 μ m spectra of a sample of 8 of the less-red and 8 of the red Jupiter Trojans. This spectral region is potentially fruitful as ices

which are seen in Kuiper belt objects have some of their strongest fundamental absorptions at these wavelengths and because dark outer main belt asteroids have been found to show some of their most distinctive absorption features in these regions (Takir & Emery 2012).

2. OBSERVATIONS AND DATA REDUCTION

We observed 16 Jupiter Trojan asteroids over a total of 8 nights from 2013 to 2015 using the facility NIRSPEC infrared medium resolution spectrograph at the Keck Observatory (Table 1). The observing procedure and data reduction were performed identically to the observations described in Brown & Rhoden (2014). In short, the target was identified by its position in the sky and by its motion with respect to background stars in short imaging exposures. The target was then placed on a 0.57 arc second wide spectral slit for a long series of nodded exposures. During this series of exposures, guiding on the target was performed using the infrared slit-viewing camera. We required two separate instrument settings to cover the range from 2.2 to 3.8 μm . At the shorter wavelength setting, which covered from approximately 2.2 to 3.1 μm at a median (2 pixel) spectral resolution, $\lambda/\Delta\lambda$, of 1600, we obtained between 18 and 40 nodded exposures, typically with 10 second integrations and 15 second coadds. For the longer wavelength setting, which covered from approximately 3.0 to 3.8 μm at a median spectral resolution of 2000, we obtained between 16 and 46 nodded exposures, typically with 1 second integrations and 150 second coadds. Beyond 3.3 μm , thermal drifts occasionally prevented high quality background subtraction. All spectra were checked by eye, and those with poor background subtraction were discarded. Correction for telluric absorption features was performed by dividing the extracted spectrum by the spectrum of a nearby solar-type star. For the two faintest Jupiter Trojans in the survey (objects 659 and 4060), the longer wavelength setting yielded no usable data, so only the short wavelength setting is used.

3. RESULTS

We first examine the brightest red and brightest less-red objects in our sample. Hektor, the largest Jupiter Trojan, is also the reddest object in our sample. Figure 1 shows the 2.2 - 3.8 μm spectrum of (624) Hektor along with a continuum extrapolation that was estimated by taking the $H - K$ synthetic photometry from Emery et al. (2011) and extending it linearly out to 4 μm . Hektor appears featureless to the level of the signal-to-noise, and the extrapolation from shorter wavelengths provides an excellent prediction of the continuum level. Patroclus, the brightest less-red object in our sample (Figure 2), in contrast, does not follow this trend. At 3 μm the flux is $\sim 10\%$ below the extrapolated continuum, and it rises well above the continuum by 3.8 μm . Smaller scale features are potentially visible, but we first chose to examine the entire data set before focusing on these features.

To highlight the broadest features of the spectra, we degrade the spectral resolution by a factor of 8 for all of the spectra by convolving each spectrum with a gaussian function with a full-width-half-maximum of 16 pixels and sampling every 8 pixels, simulating Nyquist sampled spectra with resolutions of 200 and 250 in the short and

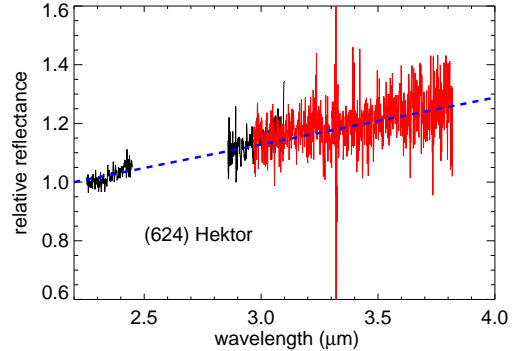


FIG. 1.— The largest Jupiter Trojan, (624) Hektor, is featureless in this wavelength range. The black and red lines show the two separate spectral settings used to cover this wavelength range, with an overlap between 2.85 and 3.1 μm . The dashed blue line is an extrapolation from the K-band spectrum of Emery et al. (2011).

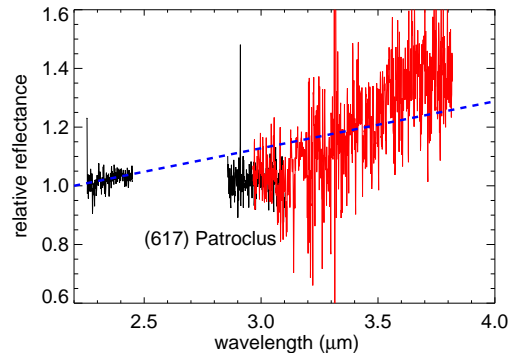


FIG. 2.— The largest less red Jupiter Trojan, (617) Patroclus, has a distinct absorption beyond 3 μm . The black and red lines show the two separate spectral settings used to cover this wavelength range, with an overlap between 2.85 and 3.1 μm . The dashed blue line is an extrapolation from the K-band spectrum of Emery et al. (2011).

long wavelength settings, respectively. Figure 3 shows these spectra for all objects, along with the extrapolation from their $H - K$ photometry. The data show that Hektor and Patroclus appear to represent two different types of spectra. The Hektor-like spectra all appear generally featureless and lie approximately along the linear extrapolation from the H-K continuum, while the Patroclus-like spectra come to a minimum at approximately 3.1 μm and rise sharply out to 3.8 μm .

To examine the relationship between the 3 μm absorption seen on some Jupiter Trojans and the two Jupiter Trojan spectral types, we construct a simple measure of the depth of the 3.1 μm feature by linearly interpolating a predicted 3.1 μm flux between the median of the data from 2.25 to 2.45 μm and the median of the data beyond 3.5 μm and then subtracting this interpolation from the measured median of the data between 3.05 and 3.15 μm . In Figure 4, we compare this 3.1 μm absorption depth to the $[\text{.85-J}]$ color from Emery et al. (2011), which they show is an excellent discriminator of the two spectral classes. For two objects, no spectral data are available beyond 3.1 μm . We find, however, that the 3.1 μm absorption depth is strongly correlated with a simple subtraction of the median of the data from 2.25 to 2.45

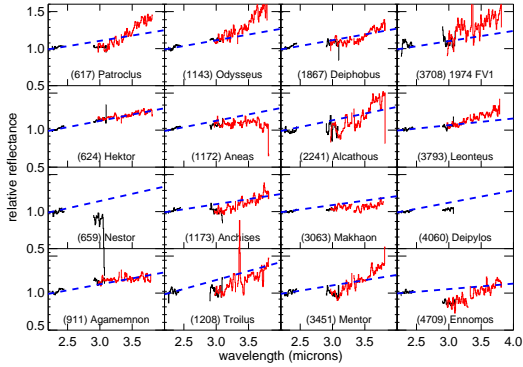


FIG. 3.— All spectra, smoothed in resolution by a factor of 8 from the original data. Some spectra appear featureless like Hector, while others show spectral features similar to that seen on Patroclus.

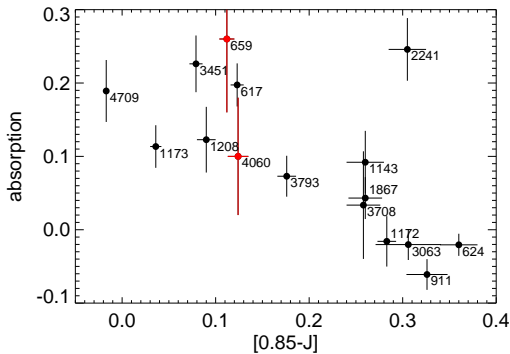


FIG. 4.— The $3.1 \mu\text{m}$ absorption depth strongly correlates with the $[.85\text{-}J]$ color for Jupiter Trojans. The less red object (defined to be those with $[.85\text{-}J] < 0.2$) all show absorption, with some of the strongest absorption on the least red objects. The red objects generally show little to no absorption, with (2241) Alcathous as a significant outlier. The objects show in red, (4060) and (659), have spectral data only out to $3.2 \mu\text{m}$ and their absorption depths have been estimated from the 2.4 to $3.1 \mu\text{m}$ ratio.

μm from the median of the data from 2.86 to $3.1 \mu\text{m}$. We estimate the uncertainties in this estimate by taking the full range of $3.1 \mu\text{m}$ absorption depths measured from objects with the same 2.3 to $3.0 \mu\text{m}$ difference.

The correlation between the $[0.85\text{-}J]$ color and $3.1 \mu\text{m}$ absorption depth is striking. A Spearman rank correlation test shows that the probability of such a high correlation due to chance is only 0.3% . Interestingly, the $3.1 \mu\text{m}$ absorption depth appears more correlated with $[0.85\text{-}J]$ color than simply bifurcated into a red and less-red group. Three objects of the red group – (3707), Deiphobus, and Odysseus – have features which appear similar to the long wavelength portion of Patroclus, while one of the red objects – Alcathous – is a clear outlier with one of the strongest $3.1 \mu\text{m}$ absorptions. The presence of a similar looking $3.1 \mu\text{m}$ absorber in both populations might be an important clue into the relationship between the less red and red populations.

4. SPECTRAL MODELING

In an attempt to understand the compositional implications of the $3.1 \mu\text{m}$ absorption, we increase the signal-to-noise by taking an average of the six spectra that show absorption depth greater than 10% . Figure 5 shows that

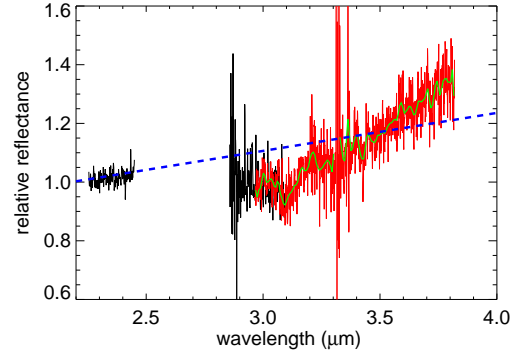


FIG. 5.— The average spectrum of the six objects with strong $3.1 \mu\text{m}$ absorption shows strong absorption from 2.9 to $3.2 \mu\text{m}$ and potential evidence of weaker absorptions beyond. The dashed line shows the averaged extrapolation of the six objects’ K-band spectra from Emery et al. (2011). The solid green line shows the average of the smoothed spectra from Figure 3.

the average of these spectra has a clear absorption with a peak depth at about $3.08 \mu\text{m}$, with reflectivity rising at longer wavelengths. A potential set of absorptions is also visible from 3.2 to $3.6 \mu\text{m}$, depending on where the continuum level is defined.

In dark asteroids, $3 \mu\text{m}$ absorption bands are often attributed to OH bands of phyllosilicates or to water ice bands (Rivkin & Emery 2010; Campins et al. 2010; Takir & Emery 2012). The decrease in reflectivity from 2.9 to $3.08 \mu\text{m}$ is the opposite of the OH phyllosilicate bands which peak in absorption in the middle of the unobserved atmospheric band and have steeply rising reflectivities from $2.9 \mu\text{m}$ onward (see the “steep” spectral type of Takir & Emery). Rather, the absorption feature appears similar to that seen in Themis (Rivkin & Emery 2010; Campins et al. 2010) and also in a small number of additional dark outer main belt asteroids (the “rounded” spectral type of Takir & Emery). On Themis, this feature has been attributed to fine grained frost covering dark silicate grains; path lengths through the water grains must be quite short in order to have such a weak absorption at $3.1 \mu\text{m}$. Our spectra can be fit with a similar model; we use an identical procedure to that used by Rivkin & Emery (2010) to model Themis and construct a Shkuratov model (Shkuratov et al. 1999) of dark grains covered with fine grained ice. The dark grains have optical constants chosen to match the albedo level of the continuum and the ice is a fine-grained frost with a volume fraction of 1.1% (chosen to match the depth of the absorption) coating the dark grains. Water ice optical constants are obtained from Mastrapa et al. (2009). The spectral fit to the $3.1 \mu\text{m}$ band is quite good (Figure 6). The continuum continues to rise at longer wavelengths, however, and broad absorption from 3.2 to $3.6 \mu\text{m}$ may also be present.

Though the fit to fine-grained water ice frost is good, we are skeptical of this interpretation for Trojan asteroids. Extremely fine grained frost is required in order to show a modest $3\mu\text{m}$ absorption while showing no hints of the shorter wavelength water ice features. While the idea that Themis, a known active asteroid, might have water vapor continuously outgassing from the interior and temporarily creating a fine grained frost seems plausible, such an interpretation for Jupiter Trojans aster-

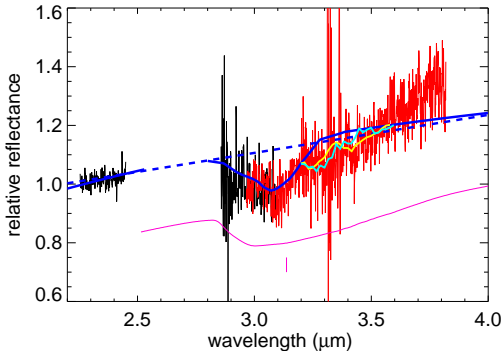


FIG. 6.— The $3.1 \mu\text{m}$ region of the spectrum of the Jupiter Trojans with features in this wavelength range can be fit by a model of dark grains covered by fine-grained water ice frost (dark blue), though we do not find such a composition to be physically plausible. The magenta line offset downward shows a laboratory spectrum of the involatile residue after the irradiation of $\text{N}_2+\text{CO}+\text{CH}_4$ ices. While much of the spectrum is dominated by water contamination, an absorption peak due to an N-H stretch, marked, appears at $3.13 \mu\text{m}$ in a location similar to the peak of the Trojan absorption. Regardless of the interpretation of the $3.1 \mu\text{m}$ region, additional absorption appears beyond $3.2 \mu\text{m}$. These absorption appears similar to those attributed to aromatic and aliphatic hydrocarbons on Saturnian irregular satellites. Phoebe (light blue) shows primarily the $3.3 \mu\text{m}$ aromatic feature, while Hyperion (yellow) shows a stronger $3.4 \mu\text{m}$ aliphatic feature.

oids seems physically unlikely. Guilbert-Lepoutre (2014) shows that water ice should be depleted to depths of $\sim 10\text{m}$ in typical Jupiter Trojan asteroids, so unusual circumstances like recent collisions would be required to have substantial active sublimation. Having such unusual circumstances in a large fraction of the Jupiter Trojan asteroids seems unlikely. We instead seek a simpler explanation for the observed absorption that does not require special circumstances. We suggest that the $3.1 \mu\text{m}$ absorption feature could be due to an N-H, rather than O-H stretch. Laboratory experiments of outer solar system ices which include nitrogen show the creation of residues with spectra similar to poly-HCN and absorptions at about $3.1 \mu\text{m}$ (Materese et al. 2014, 2015). Figure 6 shows a spectrum of electron irradiated $\text{N}_2+\text{CH}_4+\text{CO}$ from Materese et al. (2015), and while much of the $3\mu\text{m}$ region is dominated by water absorption (a contaminant in the laboratory measurement), an absorption peak at $3.13\mu\text{m}$ due to N-H appears at nearly the same location as the Trojan absorption. The laboratory experiments were not designed to specifically investigate Jupiter Trojan asteroid physical conditions and no optical constants are available to facilitate more quantitative modeling, so the lack of a perfect match is un concerning. In the context of dynamical instability models, nitrogen should indeed be present on the surface of small bodies beyond the giant planets in the form of NH_3 so it should be expected in the involatile surface mantles upon irradiation (Wong & Brown 2016). If the H_2S evaporation hypothesis of (Wong & Brown 2016) is correct, the lack of $3.1 \mu\text{m}$ absorption in most red Jupiter Trojan asteroids would mean that the presence of sulfur must disrupt much of the N-H chemistry. Such a possibility is amendable to laboratory exploration using experiments such as those performed in (Mahjoub et al. 2016).

Regardless of the spectral assignment, no known asteroid has this particular set of spectral features, though

the asteroid Themis has both a $\sim 3.1\mu\text{m}$ absorption and a set of longer wavelength absorptions that have been attributed to organic materials (Rivkin & Emery 2010; Campins et al. 2010). To search for possibly better analogs to Jupiter Trojans, we examine instead bodies from the outer solar system. The Jovian irregular satellite Himalia has a visible-to- $4 \mu\text{m}$ spectrum quite unlike any of the Jupiter Trojans, including a broad $1\text{-}2 \mu\text{m}$ absorption and a (52) Europa-like $3 \mu\text{m}$ absorption of unknown origin (Brown & Rhoden 2014). The dissimilarity between the Jupiter Trojans and Himalia is surprising, at least in the context of instability models which predict they come from the same outer solar system source population. The Jovian irregular satellites are in a significantly more intense collisional environment, however, so perhaps differences can be attributed to the effects of impacts. If so, this interpretation may have interesting implications for the other objects with (52) Europa-like spectra that reside in the asteroid belt.

The irregular satellites of the Saturnian system appear more promising. Phoebe has absorption features centered near 3.3 and $3.4 \mu\text{m}$ which have been attributed to aromatic and aliphatic hydrocarbons, respectively (Cruikshank et al. 2014). These features appear similar to those on these Jupiter Trojans asteroids. In Figure 6 we add to our spectral model a continuum-subtracted spectrum of Phoebe from 3.2 to $3.6 \mu\text{m}$. The match to the $3.3 \mu\text{m}$ absorption is good, while Phoebe's $3.4 \mu\text{m}$ absorption is not as deep as the potential feature on the Jupiter Trojans. Iapetus and Hyperion also show these spectra features, and on these the $3.4 \mu\text{m}$ feature is a closer match to that on the Jupiter Trojans. While the signal-to-noise is insufficient to definitively identify these features as aromatic and aliphatic hydrocarbon absorption features, the match with the features on the Saturnian satellites is notable.

An unusual feature of these spectra, and one that can be clearly seen even in the individual spectra of Figure 3, is that the extrapolated continuum under-predicts the reflectance beyond $3.6 \mu\text{m}$. Such behavior is not seen in the spectra of any of the dark asteroids nor in any of the small bodies in the outer solar system for which spectra are available. While this rise in flux at longer wavelengths appears similar to that expected from thermal emission, at the low temperatures of the Jupiter Trojans the thermal flux is still a small fraction of the emission at these wavelengths, and, as seen below, the flux drops at longer wavelengths.

The same reflectivity rise beyond $3.6 \mu\text{m}$ is seen in the red objects which are categorized as having a 0-10% $3.1 \mu\text{m}$ absorption in Figure 3. These objects do not show a distinct shorter wavelength band, but appear otherwise similar to the less red objects beyond $3.6 \mu\text{m}$. These objects also contain a few tantalizing features in the 2.9 to $3.1 \mu\text{m}$ range, but we deem none of them sufficiently reliable to seriously examine. The most red of the red objects, however, show no $3.1 \mu\text{m}$ absorption and no rise beyond $3.6 \mu\text{m}$.

To further explore the complete spectrum of the Jupiter Trojans, we construct mean absolute reflectances from 0.4 to $5 \mu\text{m}$ for the two spectral types (Figure 7). For the spectrum from 0.4 to $2.5 \mu\text{m}$ we use the mean red and less red spectra of Emery et al. (2011) scaled to the mean measured visible albedos from Grav et al. (2012).

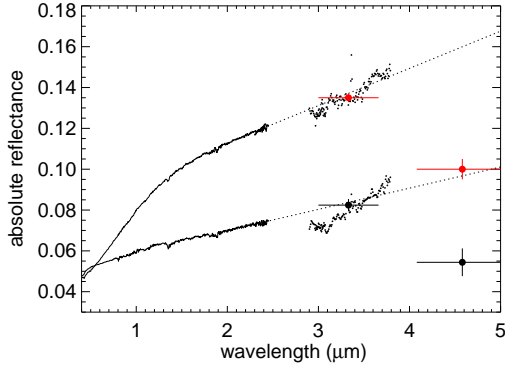


FIG. 7.— The average of the 0.4 to 5.0 μm spectral of the two spectral classes shows similarities and differences throughout the spectral range. The 0.4 to 2.4 μm data come from Emery et al. (2011), the 2.2 to 3.8 μm data are from this paper, and the two broad spectrophotometric points are from WISE photometry (Grav et al. 2012). The two red points show WISE photometry of red objects, while the two black points show WISE photometry of less red objects. No scaling is performed between the WISE data and our data; the match in the 3.5 μm band is excellent. The sharp drop in reflectivity for both the red and the less red types is the most significant feature seen in this wavelength range. Much of the structure in the 3 - 4 μm region of the red spectral type comes from adding in the single outlier (2241) Alcahous.

From 2.2 to 3.8 μm we use our average spectra for the red and less-red spectral types, scaled to match the small 2.2 to 2.5 μm overlap region. For longer wavelengths, we use average WISE reflectivities from Grav et al. (2012). The WISE observations bifurcate into the same red and less-red spectral types (Wong et al. 2014), and we use all observed objects with WISE calculated diameters greater than 80 km (at smaller diameters the uncertainties begin to dominate the measurements). We apply no scaling to the WISE reflectivities, but simply take the average absolute reflectivities measured in the 2.9 to 3.7 μm W1 band and in the 4.0 to 5.1 μm W2 band. The precise match between our extrapolated spectral reflectivities and the measured WISE reflectivities in the W1 band region is encouraging.

The sharp drop in reflectivity between the WISE W1 and W2 bands is perhaps the most surprising feature in this spectral range. The mean W2 to W1 reflectance ratio of all Jupiter Trojans larger than 80 km is 0.72 ± 0.03 . For both classes of objects, the drop in reflectivity compared to the extrapolated continuum is at least a factor of two over this $\sim 1 \mu\text{m}$ range, suggesting a broad and deep absorption. Such a broad and deep absorption in 4 to 5 μm range with no corresponding feature at shorter wavelengths has not yet been seen on any observed body in the solar system. Phoebe, for example, has a broad absorption at these wavelengths (Buratti et al. 2008), but it is due to water ice which has a very strong band at 3 μm . On these Jupiter Trojans, the at most very small water band at 3 μm predicts that no band will be detectable at 4.5 μm . The object (32532) Thereus is the only Centaur detected in both the W1 and W2 bands by WISE. The reflectivity in the W2 band is a factor of 2 *higher* than that in the W1 for this object (Bauer et al. 2013). The 3 Jovian irregular satellites that were observed in the W1 and W2 bands have a mean W2 to W1 reflectivity ratio of 1.2 ± 0.4 , which has too large of an uncertainty to allow a useful conclusion to be drawn (Grav et al. 2012).

One possibility for the low reflectivity from 4 to 5 μm is that it is caused by silicates. Dorschner et al. (1995) find that Mg rich laboratory manufactured pyroxenes glasses have spectra that can drop sharply in reflectivity beyond 4 μm . The laboratory glasses were constructed to be analogues of interstellar grains and are also representative of dust grains expected in cometary comae. Such silicate grains could also be the species responsible for the 10 μm emission detected by Emery et al. (2006) from Spitzer Space Telescope spectroscopy. Spectral modeling by Emery et al. (2011) shows that such Mg rich pyroxenes can also explain much of the red coloration of these objects.

5. DISCUSSION

Jupiter Trojan asteroids exhibit a range of 2.2 to 3.8 μm spectra strongly correlated with their optical colors. The least-red objects (and one red outlier) have distinct 3.1 μm absorptions that can be modeled as a small covering a fine-grained water ice but is also consistent with N-H stretch features seen in irradiated outer solar system ice experiments. Additional features similar to those seen and attributed to organic materials on Saturnian irregular satellites are also present. The full visible to 3.8 μm spectra most closely resemble the “rounded” 3 μm spectral type of Takir & Emery (2012). In particular, asteroids such as (153) Hilda, the largest P-type asteroid in the Hilda group, have spectra which are indistinguishable from these less-red Jupiter Trojans. The spectrum of Hilda does not have sufficient signal-to-noise beyond 3.3 μm to confirm the presence of the potential organic absorptions, but their presence cannot be ruled out.

The red Jupiter Trojans (with the exception of the single outlier) contain no detectable 3.1 μm absorption feature and no detectable organic features, but instead simply a red optical spectrum that flattens to a featureless infrared spectrum. No such spectra have been seen in the asteroids nor in the irregular satellites. The colors of the red Jupiter Trojans are indistinguishable from the colors of the red Kuiper belt objects (Tegler et al. 2008), yet these Kuiper belt objects contain sufficient amounts of water ice on their surfaces (Barucci et al. 2011; Brown et al. 2012) that they would be easily detectable as strong 3 μm absorptions on Jupiter Trojans.

The interpretation of the 3.1 μm absorption seen on the less-red Jupiter Trojans as being due to an N-H band is broadly consistent with the idea that these objects formed beyond the giant planet region, where NH_3 would have been stable, and were irradiated to form involatile residues before being emplaced at 5 AU. Wong & Brown (2016) propose that the red Jupiter Trojans formed in the outer part of the original outer disk and would have had H_2S stable on the surface during irradiation, leading to much redder colors. In this hypothesis sulfur must suppress some of the N-H chemistry, a suggestion that can be experimentally tested and, if verified, would provide strong evidence that all Jupiter Trojan asteroids formed beyond the giant planet region and that the differences in the two color populations are only due to surficial differences in ice irradiation.

An additional suggestion that the two spectral types are compositionally related comes from the observation that they both have reflectivities that drop sharply beyond 4 μm . Few species are capable of providing such a

strong absorption exclusively beyond these wavelengths, so it seems highly likely that the material causing this reflectivity drop is the same in both the red and less-red Jupiter Trojans.

Two key questions about Jupiter Trojans asteroids remain: (1) Did the two spectral classes originate from the same region? (2) Did they originate from beyond, within, or inside of the giant planet region? These data suggest the possibility that the answer to the first question is yes. Though the two populations of Jupiter Trojans asteroids are bifurcated in color, their 3-4 μm spectra form more of a continuum. Moreover, both populations contain an unusual deep spectral absorption between 4 and 5 μm . The second question remains unanswered, but confirmation of N-H absorption in the less-red objects along with verification that the presence of sulfur can mute the strength of the N-H absorption would provide powerful evidence that these objects formed in the outer solar system straddling the H_2S evaporation line, as suggested by the hypothesis of Wong & Brown (2016).

We thank Andy Rivkin and Josh Emery for illumi-

nating conversations about the nature of 3 μm absorptions in dark asteroids. Discussions with the Keck Institute for Space Studies “In Situ Science and Instrumentation for Primitive Bodies” study group, including Jordana Blacksberg, Bethany Ehlmann, John Eiler, Robert Hodyss, Ahmed Mahjoub, Michael Poston and Ian Wong have been extremely valuable to the interpretation of these data. This research was supported by Grant NNX09AB49G from the NASA Planetary Astronomy Program. The data presented herein were obtained at the W.M. Keck Observatory, which is operated as a scientific partnership among the California Institute of Technology, the University of California and the National Aeronautics and Space Administration. The Observatory was made possible by the generous financial support of the W.M. Keck Foundation. The author wishes to recognize and acknowledge the very significant cultural role and reverence that the summit of Mauna Kea has always had within the indigenous Hawaiian community. We are most fortunate to have the opportunity to conduct observations from this mountain.

REFERENCES

- Barucci, M. A., Alvarez-Candal, A., Merlin, F., Belskaya, I. N., de Bergh, C., Perna, D., DeMeo, F., & Fornasier, S. 2011, *Icarus*, 214, 297
- Bauer, J. M., Grav, T., Blauvelt, E., Mainzer, A. K., Masiero, J. R., Stevenson, R., Kramer, E., Fernández, Y. R., Lisse, C. M., Cutri, R. M., Weissman, P. R., Dailey, J. W., Masci, F. J., Walker, R., Waszczak, A., Nugent, C. R., Meech, K. J., Lucas, A., Pearman, G., Wilkins, A., Watkins, J., Kulkarni, S., Wright, E. L., WISE Team, & PTF Team. 2013, *ApJ*, 773, 22
- Brown, M. E. & Rhoden, A. R. 2014, *ApJ*, 793, L44
- Brown, M. E., Schaller, E. L., & Fraser, W. C. 2012, *AJ*, 143, 146
- Buratti, B. J., Soderlund, K., Bauer, J., Mosher, J. A., Hicks, M. D., Simonelli, D. P., Jaumann, R., Clark, R. N., Brown, R. H., Cruikshank, D. P., & Momary, T. 2008, *Icarus*, 193, 309
- Campins, H., Hargrove, K., Pinilla-Alonso, N., Howell, E. S., Kelley, M. S., Licandro, J., Mothé-Diniz, T., Fernández, Y., & Ziffer, J. 2010, *Nature*, 464, 1320
- Cruikshank, D. P., Dalle Ore, C. M., Clark, R. N., & Pendleton, Y. J. 2014, *Icarus*, 233, 306
- Dorschner, J., Begemann, B., Henning, T., Jaeger, C., & Mutschke, H. 1995, *A&A*, 300, 503
- Emery, J. P., Burr, D. M., & Cruikshank, D. P. 2011, *AJ*, 141, 25
- Emery, J. P., Cruikshank, D. P., & van Cleve, J. 2006, *Icarus*, 182, 496
- Fraser, W. C. & Brown, M. E. 2012, *ApJ*, 749, 33
- Grav, T., Mainzer, A. K., Bauer, J. M., Masiero, J. R., & Nugent, C. R. 2012, *ApJ*, 759, 49
- Guilbert-Lepoutre, A. 2014, *Icarus*, 231, 232
- Mahjoub, A., Poston, M. J., Hand, K. P., Brown, M. E., Hodyss, R., Blacksberg, J., Eiler, J. M., Carlson, R. W., Ehlmann, B. L., & Choukroun, M. 2016, *ApJ*, 820, 141
- Mastrapa, R. M., Sandford, S. A., Roush, T. L., Cruikshank, D. P., & Dalle Ore, C. M. 2009, *ApJ*, 701, 1347
- Materese, C. K., Cruikshank, D. P., Sandford, S. A., Imanaka, H., & Nuevo, M. 2015, *ApJ*, 812, 150
- Materese, C. K., Cruikshank, D. P., Sandford, S. A., Imanaka, H., Nuevo, M., & White, D. W. 2014, *ApJ*, 788, 111
- Morbidelli, A., Levison, H. F., Tsiganis, K., & Gomes, R. 2005, *Nature*, 435, 462
- Nesvorný, D., Vokrouhlický, D., & Morbidelli, A. 2013, *ApJ*, 768, 45
- Rivkin, A. S. & Emery, J. P. 2010, *Nature*, 464, 1322
- Shkuratov, Y., Starukhina, L., Hoffmann, H., & Arnold, G. 1999, *Icarus*, 137, 235
- Takir, D. & Emery, J. P. 2012, *Icarus*, 219, 641
- Tegler, S. C., Bauer, J. M., Romanishin, W., & Peixinho, N. 2008, in *The Solar System Beyond Neptune*, ed. Barucci, M. A., Boehnhardt, H., Cruikshank, D. P., Morbidelli, A., & Dotson, R., 105–114
- Wong, I. & Brown, M. E. 2015a, *AJ*, 150, 174
- Wong, I. & Brown, M. E. 2015b, in *AAS/Division for Planetary Sciences Meeting Abstracts*, Vol. 47, AAS/Division for Planetary Sciences Meeting Abstracts, 203.03
- Wong, I. & Brown, M. E. 2016, submitted
- Wong, I., Brown, M. E., & Emery, J. P. 2014, *AJ*, 148, 112

TABLE 1
LOG OF OBSERVATIONS

object	date (UT)	spectral range μm	exp. time (sec)	airmass	calibrator
(617) Patroclus	23 Nov 2013	2.2-3.1	4500	1.00-1.02	HD12846
		3.0-3.8	4000	1.00-1.02	HD12846
(624) Hektor	16 Mar 2014	2.2-3.1	2700	1.08-1.18	LHS2524
		3.0-3.8	4200	1.20-1.52	LHS2524
(659) Nestor	04 May 2015	2.2-3.1	5500	1.09-1.24	HD106116
(911) Agamemnon	02 May 2015	2.2-3.1	3600	1.56-1.63	HD111564
	01 May 2015	3.0-3.8	6900	1.56-1.70	HD111564
(1143) Odysseus	01 May 2015	2.2-3.1	3600	1.24-1.52	HD111031
		3.0-3.8	4050	1.85-1.39	HD111031
(1172) Aneas	23 Nov 2013	2.2-3.1	1800	1.21-1.37	LTT10989
		3.0-3.8	2400	1.00-1.04	LTT10989
(1173) Anchises	23 Nov 2013	2.2-3.1	2400	1.01-1.02	HD9224
		3.0-3.8	3750	1.00-1.12	HD9224
(1208) Troilus	26 Nov 2013	2.2-3.1	2700	1.00-1.03	LTT10989
		3.0-3.8	3150	1.00-1.08	LTT10989
(1867) Deiphobus	25 Nov 2013	2.2-3.1	2700	1.17-1.22	HD664
		3.0-3.8	6450	1.00-1.11	HD664
(2241) Alcahous	23 Nov 2013	2.2-3.1	1000	1.00-1.01	LHS1013
	25 Nov 2013	2.2-3.1	2700	1.06-1.14	LHS1013
	23 Nov 2013	3.0-3.8	2550	1.02-1.13	LHS1013
	24 Nov 2013	3.0-3.8	1350	1.04-1.16	LHS1013
(3063) Makhaon	02 May 2015	2.2-3.1	5400	1.50-1.54	HD132173
	03 May 2015	3.0-3.8	4200	1.49-1.62	HD132173
(3451) Mentor	24 Nov 2013	2.2-3.1	2700	1.20-1.30	HD27466
		3.0-3.8	2100	1.11-1.13	HD27466
	26 Nov 2013	3.0-3.8	2850	1.15-1.37	HD27466
(3708) 1974 FV1	26 Nov 2013	2.2-3.1	3600	1.21-1.51	LHS1428
		3.0-3.8	2700	1.03-1.16	LHS1428
(3793) Leonteus	01 May 2015	2.2-3.1	4200	1.22-1.61	HD133352
	02 May 2015	3.0-3.8	6000	1.14-1.54	HD133322
(4060) Deipylos	02 May 2015	2.2-3.1	5400	1.50-1.54	HD132173
(4709) Ennomos	25 Nov 2013	2.2-3.1	5400	1.10-1.36	LTT10989
		3.0-3.8	4050	1.01-1.07	LTT10989